Agglomeration Dynamics of 1-D Materials: Gas-Phase Collision Rates of Nanotubes and Nanorods

Adam M. Boies, Christian Hoecker, Ajinkya Bhalerao, Nikolaos Kateris, Jean de La Verpilliere, Brian Graves, Fiona Smail*

University of Cambridge, Department of Engineering, Cambridge CB2 1PZ, United Kingdom

*E-mail: a.boies@eng.cam.ac.uk (A. M. Boies)

Accepted: 23rd April, 2019

The agglomeration and self-assembly of gas-phase 1-D materials in anthropogenic and natural systems dictate their resulting nanoscale morphology, multiscale hierarchy and ultimate macroscale properties. Brownian motion induces collisions, upon which 1-D materials often restructure to form bundles and can lead to aerogels. Herein we present the first results of collision rates for 1-D nanomaterials undergoing thermal transport. The Langevin dynamic simulations of nanotube rotation and translation demonstrate that the collision kernels for rigid nanotubes or nanorods are ~10 times greater than spherical systems. Resulting reduced order equations allow straightforward calculation of the physical parameters to determine the collision kernel for straight and curved 1-D materials from 10^2-10^6 nm length. The collision kernels of curved 1-D structures increase ~1.3 times for long (>10^2 nm), and ~5 times for short (~10^2 nm) relative to rigid materials. Applications of collision frequencies allows the first kinetic analysis of aerogel self assembly from gas-phase carbon nanotubes (CNTs). The time scales for CNT collision and bundle formation (0.3-42 s) agree with empirical residence times in CNT reactors (3-15 s). These results provide insights into the CNT length, number and timescales required for aerogel formation, which bolsters our understanding of mass-produced 1-D aerogel materials.

One dimensional (1-D) rod-like structures exist in numerous natural and anthropogenic systems, where the 1-D aspect ratios of length to diameter exceed 10:1. Naturally occurring 1-D structures are found in a variety of environments, such as ice crystals[1], fibres[2] and viruses[3], and have impacts spanning from atmospheric processes to human health (see Figure 1). Synthetic 1-D materials, such as nanotubes and nanorods are of interest for a variety of industrial applications with reported synthesis of 1-D structures composed of metals, oxides, nitrides, carbides and chalcogenides.[4] 1-D material development has been motivated by superior or unique properties of these materials, such as exceptional mechanical, thermal, optical and electrical properties. Synthetically produced carbon nanotubes (CNTs), have exceptionally high thermal conductivities[5] of 3500 W/mK, electrical conductivities[6] of 2×10^7 S/m and tensile strengths[7] of 100 GPa. Silicon oxide nanowires have unique optical properties with room temperature blue light emission.[8] Aluminum nitride nanowires have high thermal conductivity (>300 W/mK)[9] with high electrical resistivity, and have deep ultraviolet emission with internal quantum efficiencies >80%.[10]

Large-scale industrial production of nanomaterials is often done via gas-phase processes, whereby material morphology is dictated by agglomeration dynamics. Gas-phase production is responsible for >90% of commercially produced nanomaterials, including nearly all carbon black and titanium dioxide each with estimated production of 5,000-10,000 tonnes annually.[11–13] Similarly, many 1-D materials are commonly synthesized by gas phase methods, such as plasma[14], laser ablation[15], flame[16] and hot-wall[17–21] reactors. Several industrial production techniques employ

gas-phase floating catalyst chemical vapor deposition (FCCVD), which allows nanorods and nanotubes to be produced in continuous flow reactors where materials are ultimately collected from the surrounding gas.[8,9,17,22–24]

During the production of nanorods and nanotubes within gas-phase reactors, the materials collide due to Brownian motion resulting in assembly of bundles and in specialized cases the bundles assemble to form networks of larger-scale structures. When the length scale of the aggregated bundle structures approach the reactor dimensions, gas-phase gelation or aerogelation[25,26] can occur whereby a macro-structure is formed from the nanomaterial components[18,27].

Aerogelation was first described by Lushnikov *et al*. in 1990 using an external electric field to cause non-spontaneous gelation of spheroidal particles.[28] Sorensen *et al.* continued this work in material synthesis systems and were the first to systematically study the phenomenon of gelation in an aerosol by demonstrating spontaneous gelation from soot particles in a laminar diffusion flame without externally applied fields. Sorensen refined the concept of aerosol gels[29,30] and gave a physical explanation of gas phase aerogelation by examining the production of an 'ultralow density porous carbon material' forming in a tubular reactor from spherical primary particles undergoing aggregation.[27,31–36] Simulation of aerogelation in 1-D systems has focused on fluid dynamics and reaction rates within such systems, but have lacked collision rates between nanotubes to determine the onset of aerogelation.[37] Industrial production of 1-D materials has focused on aerogel formation as a means to mass produce macroscopic materials formed of nanotubes composed of carbon (Tortech Nano Fibers and Nanocomp Technologies, Inc.) and boron nitride (The American Boronite Corporation). These self-assembled nanorods and nanotubes allow for the application of these unique structures to large-scale products spanning 10^{-4} to 10^{2} m.[23,38–41] While there has been significant interest in the bundling and self-assembly of nanotubes and nanorods, the unknown rate of collisions for 1-D nanomaterials prohibits the determination of timescales for agglomeration and purposeful design of reaction vessels. In the FCCVD system that motivates this study, CNTs form an aerogel network consisting of long and flexible bundles as shown in Figure 1. The CNTs form the macroscopic aerogel through a process of gas-phase rotational and translational diffusion, as well as agglomeration and reorientation upon collision whereby the rates of formation are unknown.

The collision rate $\dot{R}_{ij}$ per unit volume between the two dilute species undergoing binary collisions is given by, $\dot{R}_{ij} = \beta_{ij} n_i n_j$ where n is particle concentration and β is the collision kernel for the i, j combination.[42] While β has been determined for particles of varying size, charge and morphologies, the collision kernels for 1-D materials are unknown, which prohibits analysis of numerous atmospheric, biological, chemical and engineering systems.

Herein we report calculations of binary collision kernels for 1-D rigid and flexible nanotube and nanorod materials suspended within a gas. To determine β for distinct 1-D particles, the defining particle geometries are translated into relevant metrics for translational and rotational motion, as well as collisions. We employ Langevin dynamics to study the time scale of collision of 1-D materials and the geometry of collision relating to subsequent reorienting due to intra-particle van der Waals forces. Quantifying the range of collision kernels $\beta_{i,j}$ in gas-phase systems consisting of 1-D materials gives new insights into the spontaneous formation of aerogels from 1-D materials. These results are broadly applicable to all natural and anthropogenic 1-D materials of similar geometries undergoing gas-phase collisions.[19,43,44] As such, we employ the term nanotube generally to represent 1-D materials that may consist of nanorods, nanotubes or chain-like agglomerates with a axial length to diameter ratio >10:1.

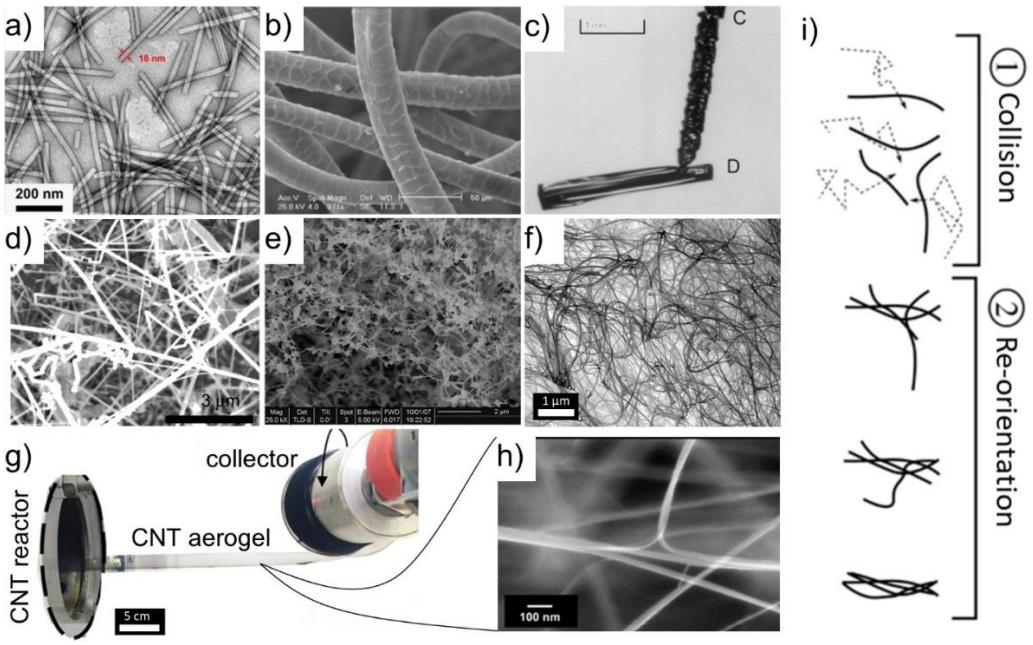

Figure 1. Microscopy images of 1-D natural materials, (a) tobacco mosaic virus[3]*, (b) wool[2]†, and (c) ice needles[1]‡, as well as aerogels of engineered materials (d) geranium nanowires[45]§, (e) boron nitride nanotubes[46]** and (f) carbon nanotubes from this group. A CNT aerogel (g) that results from collisions and entanglement of individual CNTs (h). Schematics shown on the right (i) depict the fundamental processes of 1-D nanomaterial collision and reorientation as a result of Brownian and van der Waals forces.

---

* Reprinted with permission from Liu *et al.*, Sci. Rep. 2016, 6 (1), 24567 under CC BY license.

† Reprinted with permission from Goudarzi e*t al.*, Fibres Text. 2008, 16 (3), 68 © 2008 Institute of Biopolymers and Chemical Fibres.

‡ © American Meteorological Society. Used with permission.

§ Reprinted with permission from Hanrath *et al.*, J. Am. Chem. Soc 2002. © 2002 American Chemical Society.

** Reprinted with permission from Kim *et al.*, Nano Lett. 2008, 8 (10), 3298–3302. © 2008 American Chemical Society.

RESULTS AND DISCUSSION

The collision dynamics between 1-D materials are simulated by solving the Newtonian equations of motion, known as Langevin momentum equations for translation and rotation (see SI). The non-dimensional form of the Langevin equations for translation result in a dimensionless parameter known as the diffusive Knudsen number Kn_{D}. Dahneke originally defined Kn_{D} as the ratio of the particle mean free path ℓ to a critical system lengthscale L_{C}, such that $Kn_{\mathrm{D}} \equiv \ell/L_{\mathrm{C}}$. In this context, the particle mean free path can be thought of as the length travelled by a particle undergoing Brownian motion before its motion is diverted to a direction perpendicular to the initial particle motion.[47] For particle-particle collisions, the relevant critical distance L_{C} is the collision length. The relative lengthscales follow directly from the non-dimensional form of the Langevin equations[48] as

$$Kn_{\mathrm{D}} = \left(kTm_{ij}\right)^{1/2}\pi R_{\mathrm{S},ij}/(f_{ij}PA_{ij}). \quad [1]$$

To determine the time for binary nanotube collisions, a stochastic model is developed allowing for varying nanotube lengths, which includes translational and rotational motion. The dimensionless rotational momentum equation results in an analogous term to Kn_{D} for translation, defined here as the rotational Knudsen number ($Kn_{\mathrm{D,r}}$)

$$Kn_{\mathrm{D,r}} = \left(kTI_{ij}\right)^{1/2}/(f_{\mathrm{r},ij}). \quad [2]$$

The Langevin equations are used to numerically model the translational and rotational motion of one nanotube relative to another until a collision has occurred. Upon many simulations the mean rate of nanotube-nanotube collisions can be expressed as a kernel $\beta_{\mathrm{NT},ij}$, a primary output of this work. The nanotube collision kernels are compared to well-known collision kernels for spheres, where it is expected that similar trends exist but likely at different magnitudes.[48–52] The non-dimensional collision kernel is defined in the same manner as Hogan *et al.*[52] as

$$H_{ij} \equiv \beta_{\mathrm{NT},ij}m_{ij}\pi^2 R_{\mathrm{S},ij}/(f_{ij}PA_{ij}{}^2). \quad [3]$$

These relations employ physical parameters of the colliding nanotubes, where m_{ij} is the combined nanotube mass, I_{ij} is the combined inertia, $R_{\mathrm{S},ij}$ is the combined Smoluchowski radius, PA_{ij} is the combined projected area, and f_{ij} and $f_{\mathrm{r},ij}$ are the combined friction factors for translation and rotation[53], respectively (see METHODS). The $R_{\mathrm{S},ij}$ is purely a geometrical parameter, which describes the effective combined radius for mass transfer of colliding species (also known as capacity) and can be found for arbitrarily-shaped nanotubes by known algorithms.[52,54] For a system of colliding spheres the Smoluchowski radius is equivalent to the combined radii $R_{\mathrm{S},ij} = \left(a_i + a_j\right)$ of spherical particles undergoing diffusive collisions in the continuum regime in accordance with the solution to the steady-state 1-D spherical diffusion equation, giving a collision rate of $\dot{R}_{ij} = 4\pi D_{ij}\left(a_i + a_j\right)n_i n_j$ where D_{ij} is the combined mass diffusivity. The rate of diffusive collisions between non-spherical particles is generalized as $\dot{R}_{ij} = 4\pi D_{ij}R_{\mathrm{S},ij}n_i n_j$. Likewise, the combined projected PA_{ij} is orientationally averaged projected area of the colliding species and is also found from solely geometric descriptors using numerical simulation for arbitrary shapes.[52] Expanding the analysis, the collision kernels for bent nanotubes are enabled by numerically determining their Smoluchowski radii, which allows direct calculation of the curved nanotube collision kernel.

Individual nanotubes are assumed to be composed of rigid cylinders or a series of cylindrical rod and joint segments. As is common within polymer dynamics, persistence length $P = {EI}/{k\,T}$, defines the length scale as a ratio of the bending stiffness (product of Young's modulus E and moment of inertia I) to the thermal energy of the surrounding gas (product of Boltzmann's constant k and gas temperature T), which has been a common metric reported by other groups to determine the lengthscale in which bending occurs due to the kinetic energy in the gas. Multiwall carbon nanotubes have persistence lengths up to several millimetres, whereas single wall nanotubes have persistence lengths of 32-174 μm.[55–58] Thus, for nanotubes and nanorods with persistence lengths

longer than their axial length, the materials may be treated as rigid rods. For nanotube lengths, $L_{\mathrm{NT},i}$, that exceed their persistence length, we examine their collision dynamics by modelling their structure as a series of rod and joint segments.

Figure 2 shows the resulting collision kernels for five combinations of rigid nanotube lengths, L_i which are 10^2 nm, 10^3 nm, 10^4 nm, 10^5 nm and 10^6 nm. There is strong agreement (within 25% error) between the dimensionless collision kernel H_{ij} found in this study and the reduced order relation for spheroid agglomerates given by Equation 8. As nanotube length increases Kn_D tends towards zero and in the limit of small Kn_D, $H \to 4\pi {Kn_D}^2$. While the relationship for spheroids was shown to be independent of rotational movement, the analysis of characteristic nanotube timescales of translation $\hat{t}_x$ and rotation are comparable $\hat{t}_r$, where $\hat{t}_r/\hat{t}_x$~0.3 (see Figure SI1). Including the rotation within the simulations of nanotube collisions resulted in a 5-20% increase in H_{ij} as shown in the inset of Figure 2a.

The dimensional nanotube collision kernel $\beta_{\mathrm{NT},ij}$ is plotted in Figure 2b as a function of nanotube length for the shorter length $L_{\mathrm{NT,i}}$ of the colliding nanotubes ($L_{\mathrm{NT,j}}$>$L_{\mathrm{NT,i}}$). The resulting collision kernel shows a similar form to that of the standard collision kernel for spherical particles (Chapter 13 of Seinfeld and Pandis[59]), whereby a larger length differential between colliding nanotubes results in a larger collision kernel. For long nanotubes, the system approaches the continuum limit ($Kn_{\mathrm{D}} \to 0$), $\beta_{\mathrm{NT},ij} = 4\pi \frac{kT}{f_{t,ij}} R_{S,ij}$ and at short lengths the collision kernel approaches the free molecular limit ($Kn_{\mathrm{D}} \to \infty$), $\beta_{\mathrm{NT},ij} = \sqrt{\frac{8kT}{\pi\, m_{ij}}} PA_{ij}$. Despite the similar trends to spherical particles, the 1-D nanotubes have $\beta_{\mathrm{NT},ij}$ absolute values that are nearly an order of magnitude greater than the spherical equivalent diameter for length scales greater than 10^3 nm. As shown in Figure 2b, the calculated collision kernel using the spherical relationship[59] for like-like collisions ($i = j$) is a factor of 5 to 20 lower than 1-D particles, whether treating the diameter of the particle as equal to the length of the CNT, *i.e.* $d_{\mathrm{p,i=j}} = L_{\mathrm{NT,i}}$ with $m_{\mathrm{p,i=j}} = m_{\mathrm{NT,i}}$ ($\rho_{\mathrm{p}} \neq \rho_{\mathrm{NT}}$), or using the equivalent density particle mass-based diameter, *i.e.* $m_{\mathrm{p,i=j}} = m_{\mathrm{NT,i}}$ and $\rho_{\mathrm{p}} = \rho_{\mathrm{NT}}$, thus $d_{\mathrm{p,i=j}} = \left(6\, L_{\mathrm{NT,i}}\, {R_{\mathrm{NT,i}}}^2\right)^{1/3}$. The reason for the enhanced nanotube collision kernel is seen by rearranging Equation 3, which shows a linear relationship with the dimensionless collision kernel, $\beta_{ij} \propto H_{ij}$, and quadratic relation with projected area, $\beta_{ij} \propto {PA_{ij}}^2$. The enhancement of the 1-D collision kernel when compared to spheres of the same mass and density is primarily a result of the larger projected nanotube area (*e.g.* $PA_{\mathrm{NT},10^6:10^6}$ = 4×10^{11} nm^2 and $PA_{m_{\mathrm{p,i=j}}=m_{\mathrm{NT,i}},10^6:10^6}$ = 2×10^6 nm^2). Alternatively, when comparing spheres of the same diameter as the nanotube length, the nanotube Knudsen number is 100 times larger leading to larger dimensionless collision kernel values (*e.g.* $H_{\mathrm{NT},10^6:10^6}$ = 1.5×10^{-10} and $H_{d_{\mathrm{p,i=j}}=L_{\mathrm{NT}},10^6:10^6}$ = 3×10^{-15}). The primary finding that 1-D structures have significantly enhanced collision kernels relative to compact spheres leads to increased rates of agglomeration as a result of their relatively large projected areas and diffusive Knudsen values. Plainly, nanotubes have large collision areas and their random walk is straighter between collisions than comparable spheres.

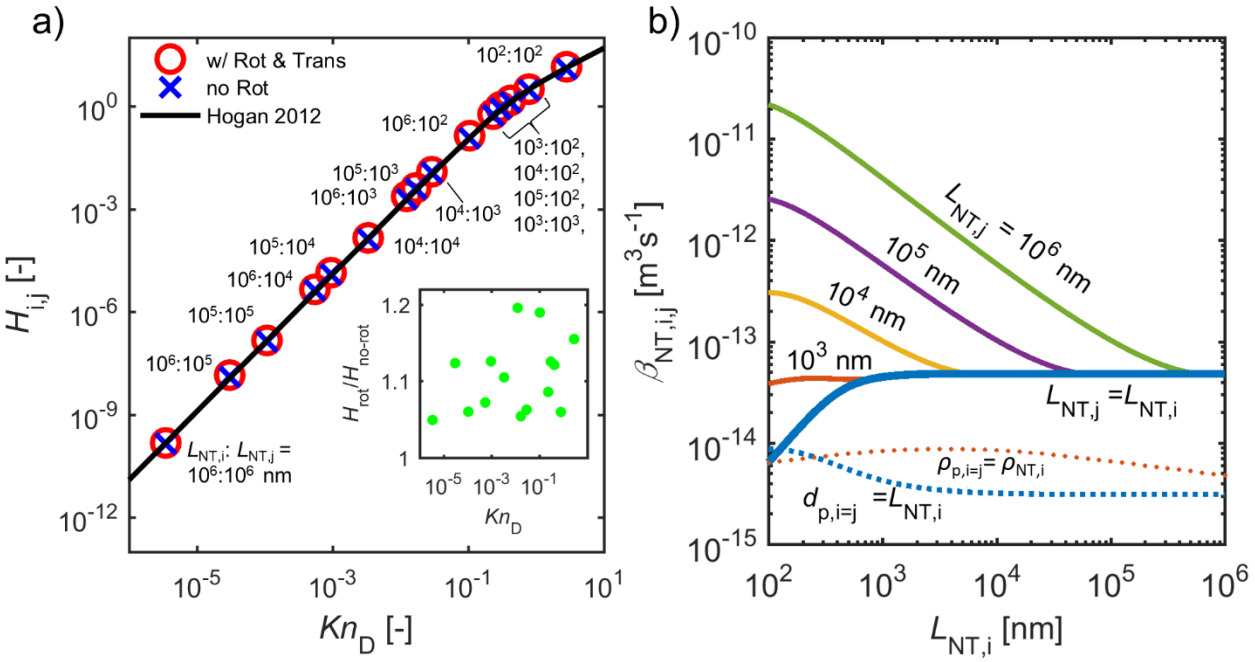

Figure 2. Nanotube collision kernel versus nanotube length scale for (a) non-dimensional kernel, $H_{i,j}$ and non-dimensional diffusive Knudsen number, Kn_D where the semi-empirical dimensionless collision kernel as a function of Kn_D is included (solid) see Equation 8. The inset depicts H as a ratio of modelled results that include nanotube rotation H_{rot} to model results where no nanotube rotation occurs H_{no-rot} (translation only). The dimensional nanotube collision kernel $\beta_{NT,ij}$ (b) as a function of nanotube length $L_{NT,i}$ is shown for paired nanotube collisions of various lengths $L_{NT,j}$, where $L_{NT,j}>L_{NT,i}$. Comparison lines (dashed) are shown for spherical particles assuming the spherical particle has an equivalent mass with diameter equivalent to the nanotube length, $d_{p,i=j}=L_{NT,j}$, as well as a spherical particles of equivalent density ($\rho_{p,i=j} = \rho_{NT,i}$).

The agreement between the modelled non-dimensional collision kernel and the semi-empirical relationship validates (<25% error) the use of Equation 8 across the range of nanotube lengths, provided the correct geometric descriptors of the 1-D materials can be determined. To obtain the dimensional collision kernel from the dimensionless relation (Equation 3) requires the calculation of combined geometric parameters of the system. The combined nanotube masses, Smoluchowski radii, friction factors and projected areas must be determined, which often require computationally expensive procedures (see METHODS). To facilitate work by others, this study developed reduced order relationships from the outputs of these simulations for the physical parameters of 1-D structures which agree to within 5% of our computationally-derived values (see Equations 4-7).

To examine the collisions between curved nanotubes, simulations composed of rod-joint structures with varying degrees of curvature at the joints were conducted. The individual Smoluchowski radii, $R_{S,i}$, (distinct from combined $R_{S,ij}$) were found for varying nanotube lengths and degrees of curvature ϕ, which was allowed to vary stochastically between successive rod segments. The angle between successive segments was chosen from a normal distribution with a mean of $\phi = 0$ and increasing standard deviations σ_ϕ, such that for $\sigma_\phi = 0$ all rods are straight and the curvature increased as the sampled distribution widened to a maximum standard deviation of $\sigma_\phi = {}^{\pi}/_{8}$. For all calculations of curved nanotubes, Figure 3a shows the mean Smoluchowski radius, μ_{R_S}, normalised by the corresponding straight nanotube Smoluchowski radius, $R_{S,straight}$..

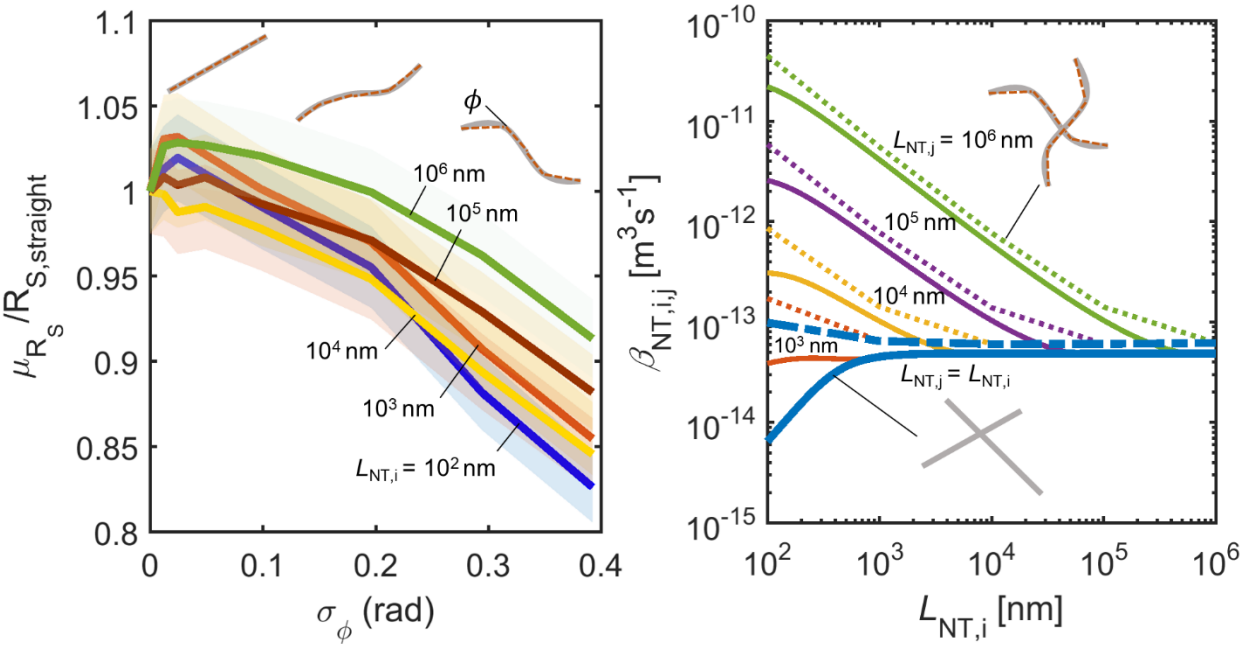

Figure 3. Individual Smoluchowski radii for bent nanotubes of lengths 10^2 to 10^6 nm with (a) mean bent Smoluchowski radii μ_{R_S} normalized by the straight radii, $R_{S,straight}$ versus the standard deviation in joint angle σ_ϕ, where shaded region represents 95% confidence interval. Collision kernel (b) versus nanotube length scale for highly curved nanotubes with $\sigma_\phi = {}^{\pi}/_{8}$ (dashed lines) compared to the straight nanotube collision kernels (solid lines).

As shown in Figure 3, the results demonstrate that as the nanotubes become increasingly curved (or bent) the Smoluchowski radius decreases. The resulting deviation in combined Smoluchowski radius is statistically significant, surpassing the 95% confidence interval (shaded region), demonstrating that as nanotubes become increasingly curved their structure is more compact (*e.g.* smaller Smoluchowski radius). Investigation of relationships between individual and combined Smoluchowski radii found no clear dependency that resulted in a reliable reduced order form, as pairs of molecules with similar individual Smoluchowski radii can result in different combined Smoluchowski radius values. Thus, the combined Smoluchowski radii must be simulated for each curved nanotube pair length and degree of curvature independently

To examine the impact of curvature on the dimensional collision kernel, the combined Smoluchowski radii were simulated for the highest value of curvature ($\sigma_\phi = {}^{\pi}/_{8}$). The resulting collision kernels were calculated using the non-dimensional semi-empirical relationship (Equations 3 and 8) as it is now shown effective for structures ranging from compact spheres to high aspect ratio 1-D structures. As shown in Figure 3b, the resulting collisions frequency of curved nanotubes is enhanced relative to nanotubes of the same length without curvature. For dissimilar nanotube lengths, the curved collision kernel is 2.6 times that of rigid 1-D structures. The enhancement due to curvature is most pronounced for short nanotubes, where the curved collision kernel has a mean value of 5 times the rigid value when at least one nanotube has a length $L_{NT} = 10^2$ nm. For longer nanotubes, both $L_{NT} > 10^2$ nm, the enhancement of the collision kernel is less pronounced with a mean enhancement of 30% for curved collisions relative to rigid. These results indicate that curvature may be important during the collision process, particularly at smaller nanotube lengths. The ultimate material curvature is dependent upon persistence length of the 1-D structures. These results likely represent an upper bound on the enhancement of curvature, where shorter nanotube lengths are unlikely to have persistence

lengths less than the length of the nanotube for all but the most flexible of materials (e.g. polymers).

Upon collision 1-D structures can reorient to reduce surface energy in a process similar to coalescence of liquid droplets for spherical aerosols. For example, CNT aerogels are composed entirely of bundles of 3-20 close-packed individual CNTs that have spontaneously assembled and reoriented as a result of surface energy minimization of the materials.[60] The bundling process is influenced by the angle and location of the collision between nanotubes, as it dictates the degree to which reorientation must occur. The collision angle and location of collision (centroid separation) were examined within the Langevin models to provide probability curves for the geometry of the collision. Figure 4a provides a schematic of the collision geometry and reorientation to a bundle along the axis normal to the minimum angle, θ, between the nanotubes. The results of the simulations demonstrate (Figure 4b) that the collision angles for all nanotube combinations were normally distributed between 0 and π, with a mean of $\pi/2$ and standard deviation of $\pi/5$. The dimensionless centroid separation, defined as $\bar{R} \equiv R/L_{\mathrm{NT,Max}}$ as shown in Figure 4c, demonstrates that for short nanotube pairs ($L_{\mathrm{NT},i=j}$ =10^2 nm) the centroid separation is larger ($\bar{R}_{\mathrm{Mode}}$ = 0.49) than larger nanotubes ($\bar{R}_{\mathrm{Mode}}$ = 0.38-0.39 for $L_{\mathrm{NT},i=j}$ = 10^3-10^6 nm). This result indicates that the shorter nanotubes are rotating faster upon approach, increasing the likelihood of a collision near the ends of the nanotube. The collision dynamics are influenced by the characteristic rotation time (see Figure SI1c), which is shorter for smaller nanotubes ($\hat{t}_r$~10^{-8} s at L_{NT} = 10^2 nm versus $\hat{t}_r$~10^{-5} s at L_{NT} = 10^3 nm) due to the lower combined inertia. The lower characteristic rotation time for shorter nanotubes results in a higher rotational Knudsen number $Kn_{\mathrm{D,r}}$ (see Table SI3). If it is assumed that the nanotubes reorient to lower surface energy along the shallowest angle between the two bodies, it is possible to determine the increased length of the resulting nanotube bundle defined as elongation $\delta = L_{\mathrm{bundle}}/L_{\mathrm{NT,Max}}$. Figure 4d demonstrates that for all like combinations the most probable elongation is δ = 1, thus no change in total bundle length due to reorientation. Elongations of δ = 2 are statistically rare, indicating that end-end collisions occur relatively infrequently and would likely result in an energetically unfavorable structure. However, as the centroid separation is greater for short nanotubes, L_{NT} < 10^3 nm, the probability of an elongation δ > 1.5 is relatively high. For nanotube collisions of dissimilar lengths (not shown), the elongation is δ ~ 1, as the contribution of the shorter nanotube to the longer length is minimal. These results provide the basis for continuum scale modelling of the collisions and reorientation of 1-D materials that can corroborate current experimental findings across a range of 1-D material systems.

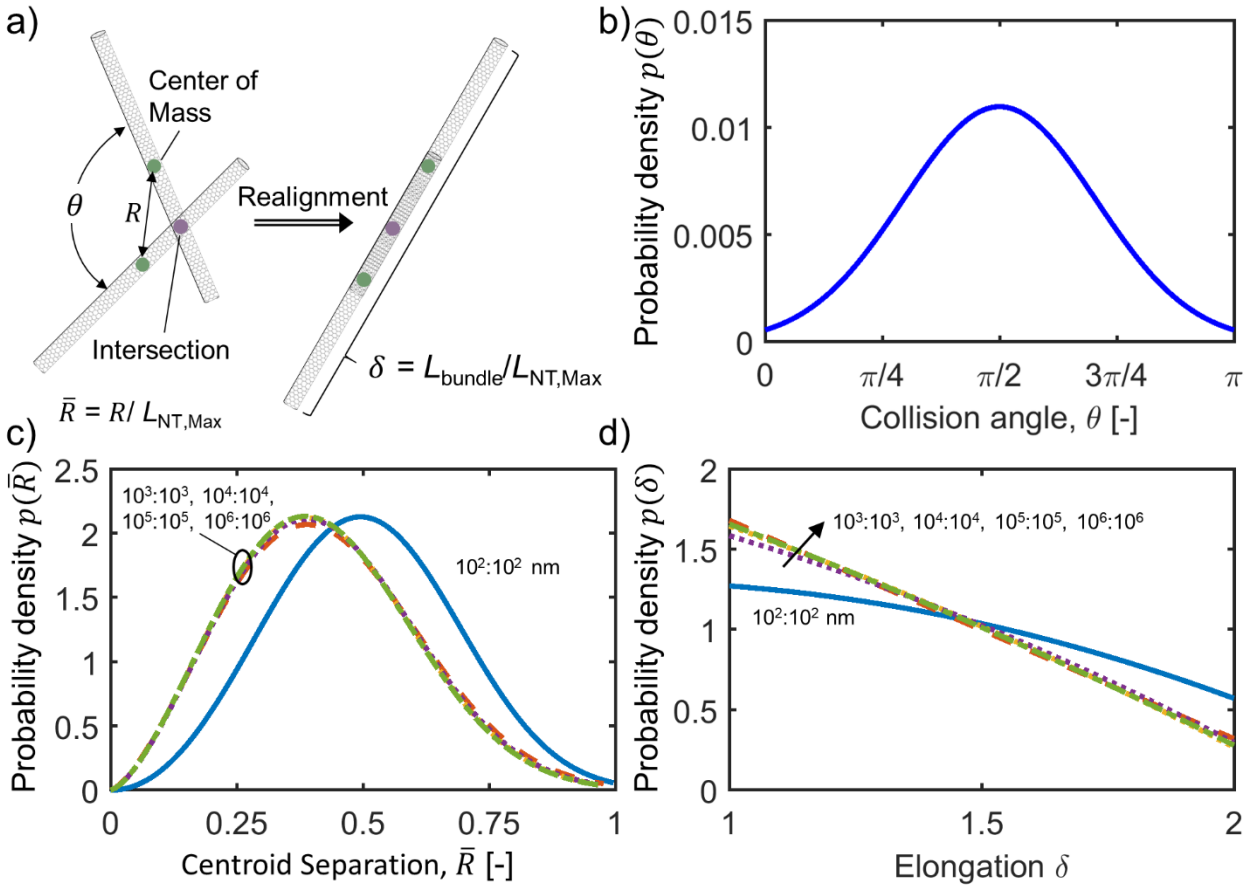

Figure 4. A schematic (a) of nanotube collision geometries and realignment defining the centroid separation R, and collision angle θ, as well as elongation θ due to realignment. The calculated probability distribution functions of (b) collision angle θ, (c) normalized centroid separation $\bar{R}$, and (d) elongation are shown for like collisions of varying nanotube lengths $L_{\mathrm{NT},i=j}$.

An application of the collision kernel for rigid 1-D materials is the process of self-assembled aerogel formation within a CNT reactor, which is of significant academic and industrial interest.[18,19,44,61] Despite the large number of studies on the nanotube aerogel process[62], the lack of known collision rates between the nanotubes has hindered quantitative understanding of the bundle formation process, a precursor to aerogel formation. Figure 5a shows the production of nanotubes and resulting self-assembled aerogel formation within a continuous gas phase chemical vapor deposition reactor. The resulting material (Figure 5b) is a hierarchical structure composed of a macroscopic aerogel at the reactor scale, composed of bundles which are formed of n_{B} = 3-20 nanotubes. The timescale for bundle formation is characterized by the well-known relation for a change in monodisperse particle number as a result collisions, $t_{\mathrm{B}} = {2(n_{\mathrm{B}} - 1)}/{\beta N_{\infty,0}}$ where $N_{\infty,0}$ is the number of individual nanotubes per unit volume prior to agglomeration.[42] The probability distribution of the number of individual nanotubes was found by stochastic calculation from the ratio of aerogel mass, volume of aerogel and mass per nanotube (see SI 1.7). The resulting mean nanotube concentration (Figure 5d) within CNT reactors at laboratory and industrial scale is $N_{\infty,\mathrm{o}} = 10^{14}$ m^{-3} [10^{13} - 10^{15} m^{-3}, 90% confidence interval]. The resulting stochastically-calculated bundling time (Figure 5e) is t_{B} = 3 s [0.2 – 42 s], which accounts for uncertainty in nanotube length, number of nanotube walls, and nanotubes per bundle among other parameters. This modelled bundling time agrees with the exogenously-

determined experimental residence times in the region where aerogels are known to form (aerogel region time) within a CNT reactor, calculated as 3 – 15 s (typically ~1/4th of total reactor residence time which is 12-60 s). As the total individual nanotube length within these reactors is uncertain (L_{NT} ~ 10^4 - 10^5 nm), Figure 5f shows the dependence on bundling time with nanotube length, accounting for the difference in collision kernels β, as well as the inverse relation (Equation SI63) between the number of nanotubes and nanotube length for a given mass of aerogel, $N_{\infty,0} \propto {L_{\mathrm{NT}}}^{-1}$. This comparison of the bundling time calculated independently from reactor parameters and the experimental reactor residence timescale, shows excellent agreement for nanotubes of lengths L_{NT} = 10^4 - 10^5 nm (dashed region). These results provide an explanation of why CNT aerogel reactors must be sufficiently large to provide residence times in excess of the minimum residence time needed for nanotube reactors to form aerogels, and highlight the impact of nanotube length and number concentration required for self-assembly.

In summary, we have provided the first known calculations of collision kernels for 1-D materials, such as nanotubes, nanorods and fibres where the aspect ratio span from 10:1 to 10^5:1. The results of the Langevin dynamics simulation that include translation and rotation, provides collision kernels for 1-D materials that can be used for continuum modelling and kinetic analysis of agglomeration. The results have been synthesized to formulate reduced order relations that provide the necessary geometric parameters for use in the non-dimensional equations, allowing direct calculation of 1-D material collision kernels without the need for further detailed simulations. The resulting collision kernels are compared to spherical particle collisions, where an enhancement of ~10 times in the collision kernel is demonstrated for 1-D rigid materials. Curved 1-D materials were found to have an enhancement of up to 5 times the collision kernel of rigid materials for short nanotubes (L_{NT} = 10^2 nm), and a 1.3 times increased kernel for longer materials (both L_{NT} > 10^2 nm). The geometry of collisions demonstrated that the nanotubes collide at greater centroid separation distances for short nanotubes (L_{NT} = 10^2 nm), as a result of the faster angular rotation. Application of the resulting collision kernels to a long-standing, but poorly understood process of nanotube aerogelation provided the first known calculation of timescales for bundle formation, which is a precursor to aerogelation. The agreement between independently calculated bundle formation time using the collision kernels and reactor residence time demonstrated the utility of well-defined collision rates. These results provide insight into the nanotube number and length required to form an aerogel, critical parameters for self-assembly. Applications of these results will enable continuum scale modelling of aerosol synthesis reactors for 1-D materials. They also allow study of other processes in which collisions between 1-D materials are important, where natural and synthetic 1-D materials, such as viruses, fibres and nanotubes, undergo agglomeration due to Brownian motion.

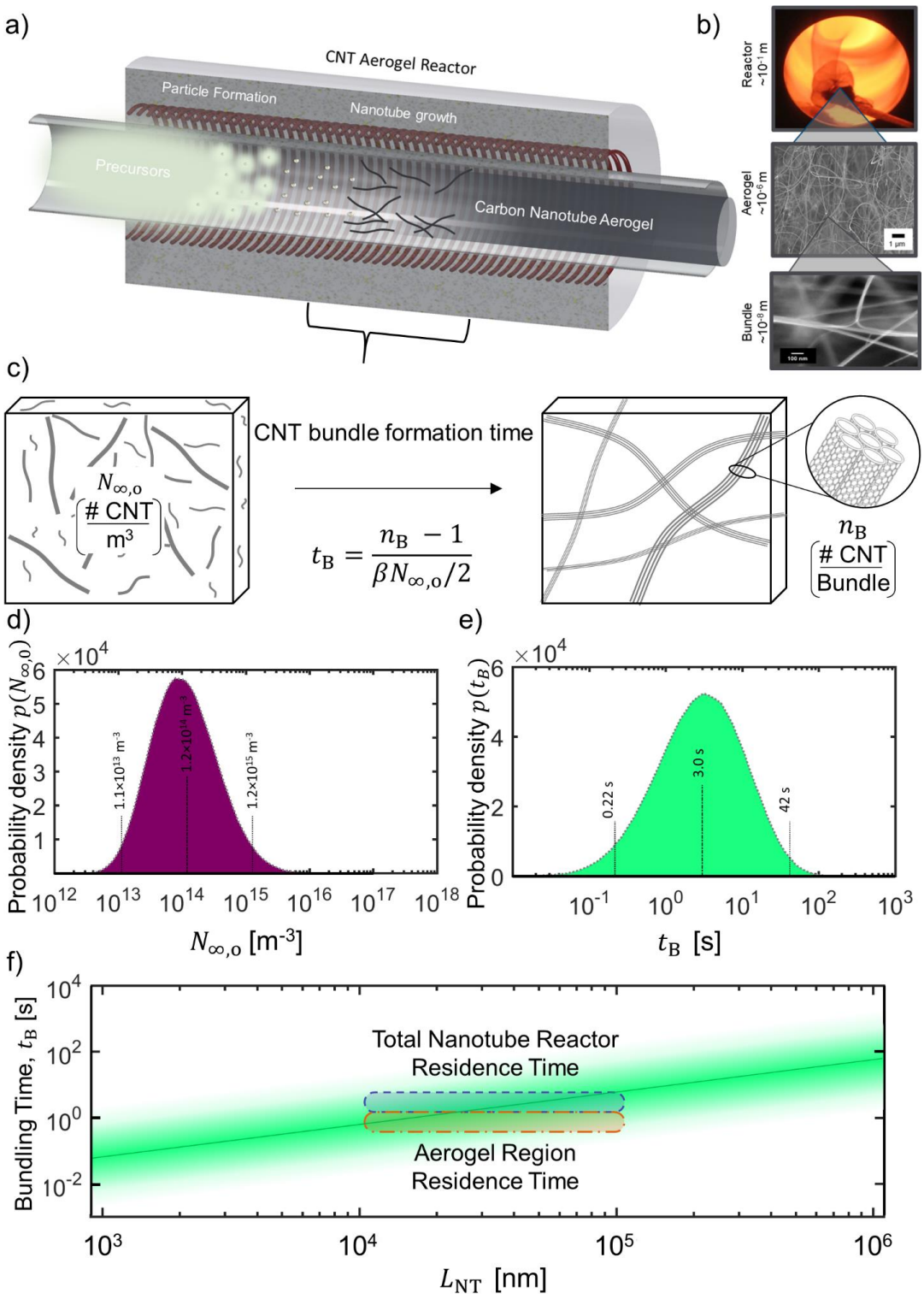

Figure 5. A diagram (a) of the CNT aerogel reactor and (b) images of the CNT product at the reactor, aerogel and bundle length scales. The bundling process (c) of the CNTs from an initial concentration $N_{\infty,0}$ of unagglomerated CNTs to bundles formed upon collision with a bundling timescale t_B as a function of the initial concentration, number of nanotubes in a bundle n_B and collision kernel. The probability density of (d) $N_{\infty,0}$ in the aerogel reactor, and (e) resulting bundling time. The bundling time (f) for varying nanotube lengths compared to total nanotube reactor residence time and aerogel region residence time.

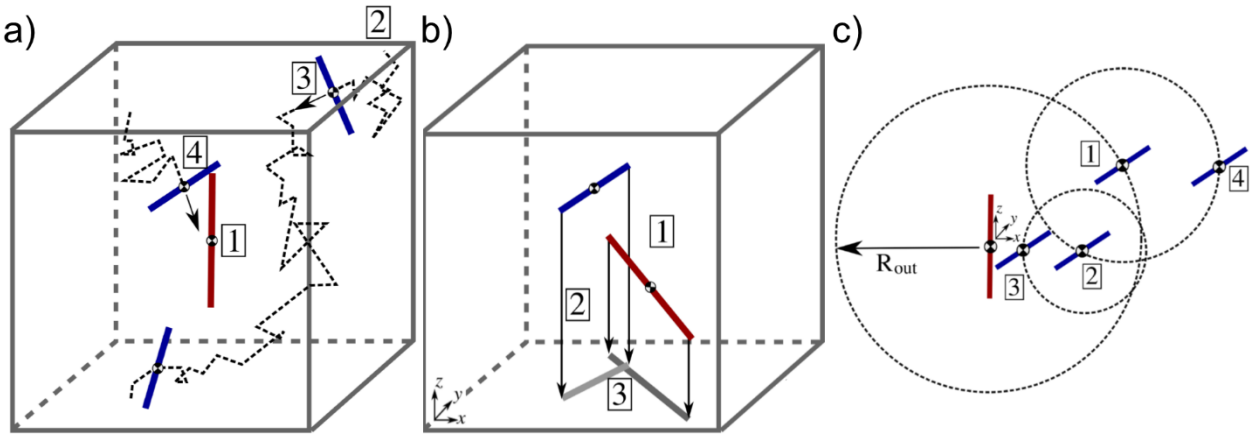

Figure 6. Schematics representing (a) the simulation of collision kernels, (b) the algorithm for calculating combined projected area and (c) the algorithm for determining Smoluchowski radius.

METHODS

The relative motion of rigid 1-D structures is modelled by a dimensionless, discretised solution to the Langevin conservation of momentum equations for translation and rotation, including thermal diffusive forces, as shown in Figure 6a. Analysis of the timescales of rotation and translation demonstrate that simulations must account for both rotation and translation, as timescales for both processes are of the same order (see SI 1.1). The magnitudes of the diffusive forces are normally distributed for translation and rotation, having zero mean and variance given by that is proportional to ${Kn_D}^2$ and ${Kn_{D,r}}^2$ (see SI 1.2).

In order to determine the required physical parameters for the collision simulation, additional algorithms were developed to determine the combined projected area PA_{ij} and Smoluchowski radius $R_{s,ij}$ for each pair of collisions. The algorithm for combined projected areas, represented in Figure 6b, combines random orientations of paired nanotubes and projects their area onto a horizontal plane (see SI 1.5). The Smoluchowski radii for paired nanotubes are modelled using diffusive first passage simulations (Figure 6c), whereby the colliding nanotube is stochastically placed on the surface of successive spheres until a collision occurs (see SI 1.6).[48,63] Using analytical expressions for combined friction factors f_{ij} and masses m_{ij}, the complete set of physical descriptors for the system allow for simulation of the dimensionless collision kernel H_{ij}. The resulting dimensional collision kernel β_{ij} is then determined from the geometry of the simulation domain (SI 1.4).

In order to facilitate future use of this study's results, reduced order relations were developed for 1-D structures that facilitate direct calculation of PA_{ij} and $R_{s,ij}$ for length ranges and aspect ratios investigated in this study. These reduced order relations take the form of equations fit with empirically or computationally derived constants that give the functional form of results output by the computational models. A relation for combined projected area is derived (SI 1.5) based on the nanotube radius R and lengths L_i and L_i,

$$PA_{ij} = \frac{\pi}{8}L_iL_j + \frac{2+\pi}{2}\left(L_i + L_j\right) + \frac{8}{\pi}R^2. \quad [4]$$

An expression for the combined Smoluchowski radius of rigid materials has be found by relation to the simulated data. Based on the nature of the $R_{S,ij}$ values the following functional form is suggested

$$R_{S,ij} = C \cdot L_{S,ij} \quad [5]$$

where $L_{S,ij}$ is the Smoluchowski radius for two lines (*i.e.* neglecting the radius) and C is a correction factor for non-slender cylinder effects. The following expressions has been developed from a non-linear least squares minimization,

$$L_{S,ij} = \frac{C_1}{L_1(\ln\psi + C_2)}, \quad [6]$$

and

$$C = C_3\xi^{C_4} + C_5\xi^{C_6}, \quad [7]$$

where $\psi = L_i/L_j$ and $\xi = \frac{2(R_1+R_2)}{\sqrt{L_1L_2}}$ is a measure of the overall non-slenderness, and C_1 = -0.5306, C_2 = -1.493, C_3 = 0.9114, C_4 = 0.005029, C_5 = 1.8, C_6 = 0.8548. The expressions in Equations 1-4 for both PA_{ij} and $R_{S,ij}$ are shown to be within 5% of simulated values (see SI 2.2).

As shown in Figure 1, the results from the simulated dimensionless collision kernel agree to within 25% with the relationship provided by Hogen *et al.*[50] for fractal-like agglomerates composed of spheroidal particles,

$$H_{ij} = \left(4\pi Kn_{\mathrm{D}}{}^2 + 25.8Kn_{\mathrm{D}}{}^3 + 11.2\sqrt{8\pi}Kn_{\mathrm{D}}{}^4\right) \Big/ \left(1 + 3.5Kn_{\mathrm{D}} + 7.2Kn_{\mathrm{D}}{}^2 + 11.2Kn_{\mathrm{D}}{}^3\right) \quad [8]$$

Dimensionless collision kernels can be computed directly for 1-D structures by combining relations provided in Equations 1 and 4-8 as well as relations for combined mass $m_{ij} = m_i m_j/(m_i + m_j)$ and friction factors $f_{\mathrm{t},ij} = f_{\mathrm{t},i} f_{\mathrm{t},j}/(f_{\mathrm{t},i} + f_{\mathrm{t},j})$, see SI 1.2. Dimensional values are then directly found from Equation 3, which are within 50% of simulated values found in this study, see Table SI3.

SUPPORTING INFORMATION

Supporting Information is provided that includes expanded methodological descriptions of the rotational and translational diffusion coefficients, Langevin dynamics, nanotube physical parameters, as well as collision kernel, projected area, Smoluchowski radius and nanotube density modelling development.

ACKNOWLEDGMENT

We would like to thank D. Seveno, L. Weller and R. Nishida for their contributions. We would like to acknowledge the support of the Engineering and Physical Research Council (EPSRC: EP/M015211/1).

REFERENCES

[1] C. A. Knight, *J. Atmos. Sci.* **2012**, *69*, 2031.

[2] Gholamreza Goudarzi, Zargham Sepehrizadeh, Mojtaba Tabatabaei Yazdi, Mostafa Jamshidiha, *Fibres Text. East. Eur.* **2008**, *16*, 90.

[3] X. Liu, F. Wu, Y. Tian, M. Wu, Q. Zhou, S. Jiang, Z. Niu, *Sci. Rep.* **2016**, *6*, 24567.

[4] C. N. R. Rao, F. L. Deepak, G. Gundiah, A. Govindaraj, *Prog. Solid State Chem.* **2003**, *31*, 5.

[5] E. Pop, D. Mann, Q. Wang, K. Goodson, H. Dai, *Nano Lett.* **2006**, *6*, 96.

[6] T. W. Ebbesen, T. W. Ebbesen, H. J. Lezec, H. Hiura, J. W. Bennett, *Nat.* **1996**, *382*, 54.

[7] B. Peng, M. Locascio, P. Zapol, S. Li, S. L. Mielke, G. C. Schatz, H. D. Espinosa, *Nat. Nanotechnol.* **2008**, *3*, 626.

[8] J. Qu, Z. Zhao, X. Wang, J. Qiu, Y. Gogotsi, *Mater. Express* **2012**, *2*, 157.

[9] Yingjiu Zhang, Jun Liu, Rongrui He, Qi Zhang, X. Zhang, J. Zhu, *Chem. Mater.* **2001**, *13*, 3899.

[10] S. Zhao, A. T. Connie, M. H. T. Dastjerdi, X. H. Kong, Q. Wang, M. Djavid, S. Sadaf, X. D. Liu, I. Shih, H. Guo, Z. Mi, *Sci. Rep.* **2015**, *5*, 8332.

[11] C. O. Robichaud, A. E. Uyar, M. R. Darby, L. G. Zucker, M. R. Wiesner, M. R, *Environ. Sci. Technol.* **2009**, *43*, 1.

[12] International Carbon Black Association (ICBA), *Carbon Black User's Guide: Safety, Health, & Environmental Information*, **2004**.

[13] F. Piccinno, F. Gottschalk, S. Seeger, B. Nowack, *J. Nanoparticle Res.* **2012**, *14*, 1109.

[14] S. I. Choi, J. S. Nam, J. I. Kim, T. H. Hwang, J. H. Seo, S. H. Hong, *Thin Solid Films* **2006**, *506–507*, 244.

[15] D. P. Yu, X. S. Sun, C. S. Lee, I. Bello, S. T. Lee, H. D. Gu, K. M. Leung, G. W. Zhou, Z. F. Dong, Z. Zhang, *Appl. Phys. Lett.* **1998**, *72*, 1966.

[16] R. L. Vander Wal, T. M. Ticich, V. E. Curtis, *Chem. Phys. Lett.* **2000**, *323*, 217.

[17] Y. Ma, A. B. Dichiara, D. He, L. Zimmer, J. Bai, *Carbon N. Y.* **2016**, *107*, 171.

[18] Y. Li, I. A. Kinloch, A. H. Windle, *Science (80-.).* **2004**, *304*, 276.

[19] C. Hoecker, F. Smail, M. Bajada, M. Pick, A. Boies, *Carbon N. Y.* **2016**, *96*, 116.

[20] T. Satake, T. Sorita, H. Fujioka, H. Adachi, H. Nakajima, *Jpn. J. Appl. Phys.* **1994**, *33*, 3339.

[21] L. Liu, W. Ma, Z. Zhang, *Small* **2011**, *7*, 1504.

[22] Y. Zhang, N. Wang, R. He, X. Chen, J. Zhu, *Solid State Commun.* **2001**, *118*, 595.

[23] Y.-L. Li, I. A. Kinloch, A. H. Windle, *Sci. (Washington, DC, United States)* **2004**, *304*, 276.

[24] T. S. Gspann, S. M. Juckes, J. F. Niven, M. B. Johnson, J. A. Elliott, M. Anne, M. A. White, A. H. Windle, *Carbon N. Y.* **2017**, *114*, 160.

[25] A. A. Lushnikov, A. E. Negin, A. V. Pakhomov, *Chem. Phys. Lett.* **1990**, *175*, 138.

[26] R. Dhaubhadel, C. S. Gerving, A. Chakrabarti, C. M. Sorensen, *Aerosol Sci. Technol.* **2007**, *41*, 804.

[27] R. Dhaubhadel, C. S. Gerving, A. Chakrabarti, C. M. Sorensen, *Aerosol Sci. Technol.* **2007**, *41*, 804.

[28] A. A. Lushnikov, A. . Negin, A. V. Pakhomov, *J. Aerosol Sci.* **1991**, *22*, 191.

[29] W. Kim, C. M. Sorensen, D. Fry, A. Chakrabarti, *J. Aerosol Sci.* **2006**, *37*, 386.

[30] C. Sorensen, W. Hageman, T. Rush, H. Huang, C. Oh, *Phys. Rev. Lett.* **1998**, *80*, 1782.

[31] C. M. Sorensen, R. Dhaubhadel, C. S. Gerving, A. Chakrabarti, *MRS Proc.* **2011**, *1306*, mrsf10.

[32] R. K. Chakrabarty, H. Moosmüller, M. A. Garro, C. B. Stipe, *Aerosol Sci. Technol.* **2011**, *46*, i.

[33] R. Dhaubhadel, F. Pierce, A. Chakrabarti, C. M. Sorensen, *Phys. Rev. E - Stat. Nonlinear, Soft Matter Phys.* **2006**, *73*, 1.

[34] W. R. Heinson, C. M. Sorensen, a. Chakrabarti, *Aerosol Sci. Technol.* **2010**, *44*, 380.

[35] R. Dhaubhadel, T. P. Rieker, A. Chakrabarti, C. M. Sorensen, *Aerosol Sci. Technol.* **2011**, *46*, 596.

[36] A. Hasmy, *J. Sol-Gel Sci. Technol.* **1999**, *15*, 137.

[37] D. Conroy, A. Moisala, S. Cardoso, A. Windle, J. Davidson, *Chem. Eng. Sci.* **2010**, *65*, 2965.

[38] K. Jiang, Q. Li, S. Fan, *Nature* **2002**, *419*, 801.

[39] H. W. Zhu, C. L. Xu, D. H. Wu, B. Q. Wei, R. Vajtai, P. M. Ajayan, *Science (80-.).* **2002**, *296*, 884.

[40] L. M. Ericson, H. Fan, H. Peng, V. A. Davis, W. Zhou, J. Sulpizio, Y. Wang, R. Booker, J. Vavro, C. Guthy, A. N. G. Parra-Vasquez, M. J. Kim, S. Ramesh, R. K. Saini, C. Kittrell, G. Lavin, H. Schmidt, W. W. Adams, W. E. Billups, M. Pasquali, W.-F. Hwang, R. H. Hauge, J. E. Fischer, R. E. Smalley, *Science* **2004**, *305*, 1447.

[41] M. Endo, T. Hayashi, Y. A. Kim, M. Terrones, M. S. Dresselhaus, *Philos. Trans. A. Math. Phys. Eng. Sci.* **2004**, *362*, 2223.

[42] S. K. Friedlander, *Smoke, Dust, and Haze: Fundamentals of Aerosol Dynamics*, Oxford University Press, New York, **2000**.

[43] C. Hoecker, F. Smail, M. Pick, A. Boies, *Chem. Eng. J.* **2017**, *314*, 388.

[44] C. Hoecker, F. Smail, M. Pick, L. Weller, A. M. Boies, *Sci. Rep.* **2017**, *7*, DOI 10.1038/s41598-017-14775-1.

[45] T. Hanrath, B. A. Korgel, *J. Am. Chem. Soc* **2002**, *124*, 1424.

[46] M. J. Kim, S. Chatterjee, S. M. Kim, E. A. Stach, M. G. Bradley, M. J. Pender, L. G. Sneddon, B. Maruyama, *Nano Lett.* **2008**, *8*, 3298.

[47] B. Dahneke, *Theory Dispersed Multiph. Flow. Proc. an Adv. Semin.* **1983**, 97.

[48] R. Gopalakrishnan, T. Thajudeen, C. J. Hogan, **2011**, *135*, DOI 10.1063/1.3617251.

[49] R. Gopalakrishnan, C. J. Hogan, *Phys. Rev. E - Stat. Nonlinear, Soft Matter Phys.* **2012**, *85*, 1.

[50] R. Gopalakrishnan, C. J. Hogan, *Aerosol Sci. Technol.* **2011**, *45*, 1499.

[51] T. Thajudeen, S. Deshmukh, C. J. Hogan, *Aerosol Sci. Technol.* **2015**, *49*, 115.

[52] T. Thajudeen, R. Gopalakrishnan, C. J. Hogan, *Aerosol Sci. Technol.* **2012**, *46*, 1174.

[53] S. H. Kim, G. W. Mulholland, M. R. Zachariah, *J. Aerosol Sci.* **2007**, *38*, 823.

[54] H.-X. Zhou, A. Szabo, J. F. Douglas, J. F. Douglas, J. B. Hubbard, *J. Chem. Phys.* **1994**, *100*, 3821.

[55] H. S. Lee, C. H. Yun, H. M. Kim, C. J. Lee, *J. Phys. Chem. C* **2007**, *111*, 18882.

[56] W. Zhou, M. F. Islam, H. Wang, D. L. Ho, A. G. Yodh, K. I. Winey, J. E. Fischer, *Chem. Phys. Lett.* **2004**, *384*, 185.

[57] R. Duggal, M. Pasquali, *Phys. ReV. Lett.* **2006**, *96*, 1.

[58] N. Fakhri, D. a Tsyboulski, L. Cognet, R. B. Weisman, M. Pasquali, *Proc. Natl. Acad. Sci. U. S. A.* **2009**, *106*, 14219.

[59] J. H. Seinfeld, S. N. Pandis, *Atmospheric Chemistry and Physics: From Air Pollution to Climate Change*, John Wiley & Sons, **2016**.

[60] J. C. Stallard, W. Tan, F. R. Smail, T. S. Gspann, A. M. Boies, N. A. Fleck, *Extrem. Mech. Lett.* **2018**, *21*, 65.

[61] C. Hoecker, F. Smail, M. Pick, A. Boies, *Chem. Eng. J.* **2017**, *314*, 388.

[62] L. Weller, F. R. Smail, J. A. Elliott, A. H. Windle, A. M. Boies, S. Hochgreb, *Carbon N. Y.* **2019**, DOI 10.1016/J.CARBON.2019.01.091.

[63] I. Chan Kim, S. Torquato, *J. Appl. Phys.* **1991**, *69*, 2280.